Available online at www.sciencedirect.com

SCIENCE DIRECT®

Earth and Planetary Science Letters 226 (2004) 193–205

EPSL

www.elsevier.com/locate/epsl

Geomagnetic effects on time-integrated cosmogenic nuclide production with emphasis on in situ ^{14}C and ^{10}Be

Jeffrey S. Pigati*, Nathaniel A. Lifton

Department of Geosciences, University of Arizona, Gould-Simpson Building, 1040 E. Fourth St., Tucson, AZ 85721-0077, United States

Received 14 January 2004; received in revised form 30 June 2004; accepted 19 July 2004
Editor: K. Farley

Abstract

Production of cosmogenic nuclides (CNs) in geologic material is a function of the cosmic-ray flux at the Earth's surface, which in turn is a function of the intensity and orientation of the Earth's geomagnetic field. Temporal variations in the intensity of the geomagnetic field and the position of the geomagnetic dipole axis (i.e., polar wander) must be considered when calculating production rates that are integrated through time. We have developed a model, based in part on protocols set forth by Desilets and Zreda [Earth Planet. Sci. Lett. 206 (2003) 21–42], that accounts for these variations in an effort to systematically determine their impact on time-integrated production of short-lived (in situ ^{14}C; $t_{1/2}$=5.73 ka) and long-lived (in situ ^{10}Be; $t_{1/2}$=1.5 Ma) CNs. Our modeling results show that for samples exposed for the last 3 ka, integrated in situ ^{14}C and ^{10}Be production rates that account for temporal variations in the intensity of the Earth's geomagnetic field are up to ~13% lower than modern rates at the same location [modern rates are referenced to the 1945.0 Definitive Geomagnetic Reference Field (DGRF)]. In contrast, intensity-corrected ^{10}Be rates are up to ~30% higher than modern for samples exposed for >25–30 ka. Intensity variations have little effect (<5%) on integrated CN production for samples exposed for the last 15–20 ka, regardless of site location or nuclide used.

Our modeling results also show that the impact of polar wander on integrated CN production is secondary compared to intensity variations. Accounting for polar wander is critical, however, when determining modern production rates at midlatitudes (30–40°) because of the current offset between the geomagnetic and geographic poles. At sea level, integrated in situ ^{14}C production rates that account for both intensity variations and polar wander range from 27% higher to 24% lower than modern rates at the same location, and integrated in situ ^{10}Be rates range from 48% higher to 26% lower than modern. Differences between integrated and modern rates increase significantly at higher altitudes. Based on these results, we recommend correcting the modern production rate (referenced to the 1945.0 DGRF or another specific geomagnetic reference field) at site latitudes <60° for variations in the intensity of the Earth's geomagnetic field during exposure and for polar wander over the last 10 ka.

Keywords: surface exposure dating; production rates; geomagnetic field; paleointensity; polar wander

* Corresponding author. Tel.: +1 520 621 6024; fax: +1 520 621 2672.
E-mail address: jpigati@geo.arizona.edu (J.S. Pigati).

0012-821X/$ - see front matter © 2004 Elsevier B.V. All rights reserved.
doi:10.1016/j.epsl.2004.07.031

1. Introduction

Production of in situ cosmogenic nuclides (CNs) in geologic material is a function of the flux of cosmic radiation that reaches the Earth's surface. The cosmic-ray flux has varied through time due to (1) variations in the primary galactic cosmic ray (GCR) flux, (2) solar modulation of the GCR flux, (3) changes in atmospheric shielding, and (4) variations in the intensity and orientation of the Earth's geomagnetic field. The impact that each of these has on geologic applications of in situ CNs depends primarily on the time scale on which it operates. Most cosmogenic-based research to date has focused on surficial processes that operate on time scales in the 10^3 to 10^5 year range (e.g., bedrock and basin-wide erosion [2–5], glacial processes [6–8], volcanic eruptions [9,10], and paleoseismicity [11,12]). Low frequency (>10^6 years) variations, such as (1), and high frequency (10^0 to 10^2 years) variations, such as (2), have minimal influence on CN production integrated over 10^3 to 10^5 years. Even exceptionally powerful short-lived events, such as supernovae, do not generally affect CN production rates because production is usually integrated over long periods of time [13].

Changes in atmospheric shielding through time may be important for determining integrated CN production rates [14], particularly for areas where atmospheric conditions fluctuate with periods similar to or exceeding the application time scale. However, atmospheric pressure is not recorded by any known proxy system, thereby limiting pressure data to historical records. Global circulation models (GCMs) have certainly improved over the last decade, but still lack the accuracy and resolution necessary to constrain atmospheric conditions to the level required to determine their effect on CN production through time. Until proxy records for reconstructing atmospheric conditions are developed and/or GCMs improved, CN production rates must be calculated using either historically averaged local atmospheric pressure data (corrected to sea level) or the standard sea-level pressure value (applied globally) in concert with an atmospheric model.

The primary source of temporal variability in CN production that can be addressed adequately is the Earth's geomagnetic field. Independent proxy records are available that document changes in both the geomagnetic field intensity [15–17] and the position of the geomagnetic dipole axis (or geomagnetic pole) [18–21] through time. Models have been developed previously to determine the impact that these variations have on production of longer-lived and stable CNs (e.g., [13,22–27]). However, discrepancies between models and the lack of a systematic evaluation of the impact of geomagnetic variations on CN production, particularly for short-lived CNs, have left it unclear as to when and where geomagnetic variations must be taken into account.

We have developed a model, based in part on protocols set forth by Desilets and Zreda [1], to quantify the effects that temporal variations in the Earth's geomagnetic field have on time-integrated production of both short-lived (in situ ^{14}C; $t_{1/2}$=5.73 ka) and long-lived (in situ ^{10}Be; $t_{1/2}$=1.5 Ma) CNs (Appendix A). Our model differs significantly from some recent models in that integrated production rates are normalized to the modern production rate at the *geomagnetic*, rather than *geographic*, latitude of a given site. Normalizing integrated production rates to the modern rate at a site's geographic latitude incorrectly suggests that a single correction can be applied to all sites along a given parallel (e.g., Fig. 6 in [26]; Fig. 3 in [27]). In contrast, integrated production rates normalized to the modern rate at a site's geomagnetic latitude explicitly account for the fact that modern production reflects the current offset between the geomagnetic and geographic poles, and that time-integrated production is affected by polar wander differently at different locations [13]. For these reasons, we referenced all geomagnetic latitudes in our model to the 1945.0 Definitive Geomagnetic Reference Field (DGRF; http://www.ngdc.noaa.gov/IAGA/vmod/igrf.html). We selected this reference field because its time frame approximately coincides with the rapid expansion of instrumental measurements of atmospheric cosmic radiation (e.g., [28]), although any reference field would suffice as long as a specific field is adopted for use by the entire CN research community.

2. Influence of geomagnetic field variations on CN production

Primary GCRs are composed of particles that originate outside our solar system, but are thought to

come from within the Milky Way galaxy [29]. These particles, consisting of 87% protons, 12% α-particles, and 1% heavy nuclei, are highly energetic, with the vast majority falling between ~0.1 and 10 GeV [30,31]. After passing through interplanetary and terrestrial magnetic fields and intercepting the Earth's atmosphere, primary GCRs initiate nuclear reactions that generate cascades of secondary particles that can ultimately produce in situ CNs in the upper few meters of the Earth's crust.

The primary GCR flux is thought to be essentially isotropic outside the solar system (e.g., [32]). However, particle fluxes inside the solar system are heavily influenced by magnetic fields carried by the solar wind (e.g., [33]). Closer to Earth, the geomagnetic field is the dominant influence on the trajectories of primary GCRs. Charged primaries are admitted or rejected by the geomagnetic field based on their rigidity R (momentum per unit charge, in units of GV) and angle of incidence. For a given angle of incidence at a given location, the rigidity of an incoming primary GCR particle must exceed the cutoff rigidity (R_c) value at that location in order to penetrate the Earth's magnetic field and reach the upper atmosphere. For computational simplicity, R_c has typically been restricted to vertically incident particles (i.e., vertical cutoff rigidity) when studying the geographic distribution of cosmic radiation (e.g., [34])—we follow that convention here. For a dipolar geomagnetic field, R_c values are highest at the cosmic-ray equator, where the magnetic field lines essentially parallel the Earth's surface, and decrease toward the geomagnetic poles as the field lines become more vertical. Incoming primaries with rigidities below the R_c are deflected either back to space or toward higher geomagnetic latitudes. At latitudes greater than ~55°, the R_c falls below the minimum rigidity present in the primary flux, and all primaries are admitted.

The long-term average geomagnetic field is typically assumed to be a geocentric axial dipole (GAD), in which the dipole axis coincides with the Earth's rotational axis. In such a case, the cosmic ray and geographic equators coincide and the equatorial R_c value is ~14.9 GV (referenced to the 1945.0 DGRF) [35]. The modern geomagnetic field consists of an eccentric dipole (its axis does not pass through the center of the Earth) and nondipole components that distort the geomagnetic field away from that of a pure dipole. In fact, the nondipole field may comprise up to 10–25% of the total field strength at a given location over brief periods of time [26]. However, nondipolar components tend to be transient in time and space, as is the eccentricity of the dipole, and a geocentric dipole appears to be a reasonable first-order approximation over periods of 10^3 to 10^5 years.

Secondary nucleons (neutrons and protons) and mesons (kaons, muons and pions) are produced in the upper atmosphere during collisions between primary GCRs and various targets, including atmospheric gas nuclei and a range of subatomic particles. While the spectra of the primary and secondary fluxes are similar in the upper atmosphere [i.e., atmospheric depths <100 g cm^{-2} or altitudes >16 km above sea level (ASL)], the secondary flux diminishes with increasing atmospheric depth approximately exponentially as the nuclear cascade loses energy through successive collisions [13]. The composition of the secondary flux also changes with increasing atmospheric depth as neutrons become dominant over protons [36].

The interaction between the cosmic-ray flux and the geomagnetic field causes CN production to decrease with decreasing latitude, such that sea-level production by high-energy nucleons at the equator is approximately half of the production at high latitudes. Production rates have been determined for several CNs at a handful of calibration sites worldwide, and models have been developed to scale production rates from calibration sites to sea level and high geomagnetic latitude (SLHL; by convention), and then back to sites of geologic interest [1,14,26,37,38]. For a given in situ CN, the cosmic-ray particles contributing to its production (e.g., high-energy and slow nucleons, fast and slow muons) should be scaled separately due to differing altitude–latitude distributions for each particle type [1].

3. Records of temporal changes in the Earth's geomagnetic field

Temporal variations in the intensity and orientation of the geomagnetic field must be considered when calculating time-integrated CN production rates. As a basis for developing a consistent procedure of accounting for these variations, we discuss below our rationale for choosing specific geomagnetic

records and describe our treatment of the geomagnetic data in detail.

Several types and sources of paleomagnetic data can be used to quantify variations in the geomagnetic field over the recent geologic past (Holocene and late Pleistocene), as well as deeper in time [35]. Sources that have been used previously include remanent magnetization (RM) in archeomagnetic materials, volcanic flows, and sediment cores (e.g., [15–18,39]), $\Delta^{14}C$ in tree rings [27], and meteoric ^{10}Be in marine sediments [40,41]. For this study, we avoided using atmospheric-based paleomagnetic records, specifically atmospheric ^{14}C, for two reasons. First, atmospheric ^{14}C is preferentially produced at high latitudes (~30% is produced at >60° latitude; [30]) where changes in the geomagnetic field intensity do not affect production rates. Atmospheric ^{14}C produced at high latitudes quickly mixes with ^{14}C produced elsewhere, which results in a diluted, globally averaged signal that underestimates the magnitude of intensity variations at a specific site. For example, if the geomagnetic field intensity doubled, production of in situ cosmogenic ^{14}C at sea level at the equator would decrease by ~35%, whereas the ^{14}C activity of atmospheric CO_2 would decrease by only ~21% (calculated from Table 1 and Fig. 10b of [30]). Meteoric ^{10}Be is subject to similar dilution effects and is further complicated by the fact that it is transported from the atmosphere to the ground surface by precipitation, aerosols, and dust [41]. These transport mechanisms are not homogeneously distributed across the globe and, therefore, spatial patterns of meteoric ^{10}Be reconstructed from sediment cores are not necessarily identical to spatial patterns of ^{10}Be production in the atmosphere.

Second, reconstructions of past geomagnetic field conditions based on atmospheric ^{14}C (typically as $\Delta^{14}C$) must account for exchange of carbon between the atmosphere and ocean, as well as other smaller reservoirs. While this can be done using a box model (e.g., [42–44]), it adds additional and unnecessary uncertainties that can be avoided by using more direct paleomagnetic records, such as RM. On the other hand, ignoring exchange of ^{14}C between reservoirs, even during relatively quiescent periods such as the Holocene, can lead to a significant underestimation of the actual paleomagnetic variations [45]. For example, Masarik et al. [27] used the INTCAL98 atmospheric ^{14}C calibration curve [46] to derive a paleomagnetic record for the last 10 ka, apparently without using a box model. Although their paleomagnetic record features changes that are in the same directions as those reconstructed from RM data [17], the atmospheric ^{14}C production signal embedded in INTCAL98, and the resulting paleomagnetic record, is damped and diluted by at least an order of magnitude. This damping effect is well known and is the primary reason that researchers modeling the ^{14}C paleorecord (e.g., [44]) use RM data as model input.

For this study, we relied on a compilation of thermoremanent magnetization (TRM) data in archeomagnetic material to constrain changes in geomagnetic field intensity during the Holocene, postdepositional remanent magnetization (post-DRM) data in stacked marine sediments to constrain field intensity changes in deeper time, and TRM data from archeomagnetic material and post-DRM in terrestrial sediments to constrain the position of the geomagnetic pole through the Holocene. Each of these sources has important requirements and limitations, discussed below, which must be appreciated when evaluating their impact on time-integrated CN production. One requirement common for all sources is that the paleomagnetic data must be placed in a firm chronologic framework. This is particularly important when integrating or stacking paleomagnetic records because the tie points are often based on the chronologic data. A second common requirement is that the paleomagnetic records be distributed as evenly as possible around the world. Global coverage minimizes geographical biases within the data, which can arise from the nondipole component of the geomagnetic field or when the geomagnetic pole does not coincide with the Earth's rotational axis [35].

3.1. Geomagnetic field intensity

3.1.1. Archeomagnetic data

Geomagnetic field intensity information can be obtained from fired ceramic material recovered from surficial settings at open-air archeological sites or found in situ during excavations. TRM is locked in ceramics when the fired material cools below the Curie temperature, which preserves a nearly instantaneous record of magnetic field intensity [35]. The quality of archeointensity data is determined by the

presence and preservation of appropriate mineral phases, the quality of the independent age control for each site, and the number and distribution of sites for a given time period.

Yang et al. [17] analyzed a compilation of archeointensity data (a total of 3243 records) that span the last 12 ka and cover much of the Northern Hemisphere. Their data set improves upon a previous compilation [39] by expanding geographical coverage outside of Europe, particularly in Asia. For each site, measured geomagnetic field intensity data were transformed to virtual axial dipole moment (VADM) values, which were averaged over periods of 0.5–1 ka to eliminate the influence of nondipole field variations.

3.1.2. Marine sediment data

Changes in the intensity of the Earth's geomagnetic field in deeper time, up to 800 ka BP, are recorded in the post-DRM of marine sediments [15,16]. Small mineral grains that are magnetized during their predepositional history are able to move freely within the water-filled interstices of newly deposited sediment. As the sediment becomes compacted, the magnetic axes of the minerals align with the ambient magnetic field and are eventually locked into position, giving the sediment an overall magnetization that is parallel to the Earth's geomagnetic field [35]. Although measuring the RM along a sediment core is relatively straightforward, the interpretation of post-DRM in sediments has been debated (i.e., is it a geomagnetic or paleoenvironmental signal?). Guyodo and Valet [15] argued that post-DRM in marine sediments is solely the result of geomagnetic processes based on the coherency between records obtained from a variety of paleoenvironmental conditions, lithologic contexts, and sedimentation rates. However, even if magnetization in marine sediments is indeed solely the result of geomagnetic processes, there may be additional complications in reconstructing paleointensity variations from sediments. These include (1) the age of acquisition may not coincide with the timing of sediment deposition, particularly for areas with low deposition rates, (2) paleointensity variations are smoothed during the acquisition process, and may be smoothed even more by turbation or mixing of sediments after deposition, and (3) disturbance or deformation of the sediments during the coring process may be difficult or impossible to detect.

Guyodo and Valet [16] integrated 33 records of paleomagnetic intensity that are reasonably well distributed: 5 records from high latitudes (>40°), 8 records from midlatitudes (16–40°), and 20 records from low latitudes (0–15°). Relative VADMs were calculated after the measured RM data were normalized by a magnetic parameter that activates the same magnetic fraction as that which carries the RM ([16]; p. 250). The relative VADM values were then divided by the mean VADM value of the core to allow integration of the records on a common scale. Chronologic control was based on wiggle-matching $\delta^{18}O$ data obtained from planktonic foraminifera in each of the marine cores to reference oxygen isotope curves (e.g., [47]).

Integrated VADM values for each time period were converted to absolute values by calibration with TRM from archeomagnetic material [39] and natural remanent magnetization (NRM) data from volcanic flows in New Zealand, Japan and western Europe [48,49].

3.1.3. Treatment of geomagnetic field intensity data

Archeomagnetic and marine sediment records of the paleointensity of the Earth's geomagnetic field were originally reported in units of A m^{-2} [15–17]. We normalized these reported values (M) by dividing by the intensity of the magnetic field in 1945 (8.075×10^{22} A m^2; M_0; 1945.0 DGRF). Archeointensity data were reported at 0.5-ka time intervals for the past 4 ka, and at 1-ka time intervals between 4 and 12 ka [17]. Paleointensity data from marine sediments were reported at 1-ka time intervals between 2 and 800 ka [15,16]. We did not combine the two data sets where they overlap because the records are not independent (the archeomagnetic data were used to calibrate the relative VADM values from the marine sediment). Instead, we used the archeomagnetic data exclusively for the last 12 ka and the marine sediment data beyond that. The combined paleointensity records for the last 60 ka are shown in Fig. 1.

3.2. Variation in the geomagnetic pole position

3.2.1. Archeomagnetic data

Temporal variations in the position of the geomagnetic pole can be reconstructed using the TRM of archeomagnetic material if the fired material has not

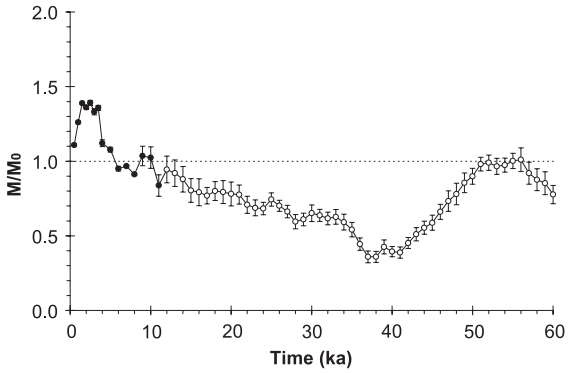

Fig. 1. Combined archeomagnetic and marine sediment paleointensity record for the last 60 ka. Archeomagnetic data from Yang et al. [17] are shown as filled circles; marine sediment data from Guyodo and Valet [16] are shown as open circles; modern intensity (M/M_0=1) indicated by dashed line. Uncertainties are given as standard error of the mean at the 1σ level.

been disturbed since cooling. Such conditions are met more frequently for bricks that line pottery kilns and ancient fireplaces than in ceramic pottery itself [35]; these have been used to reconstruct the position of the geomagnetic pole over the past 2 ka [18,19]. These studies compiled TRM data from eight arbitrarily chosen regions around the world. Within each region, a virtual geomagnetic pole (VGP) position was calculated at 100-year time intervals. VGP data from all eight regions were then averaged for each time interval to minimize the effects of nondipole field fluctuations. Merrill and McElhinny [19] contend these methods yield accurate VGP positions because (1) the mean VGP calculated from the 1980 field values for the center of each of the eight regions is close to the position of the 1980 geomagnetic pole, (2) the calculated VGP position derived from archeomagnetic material is consistent with historical observations, and (3) the scatter in VGPs remains relatively constant through time.

3.2.2. Terrestrial sediment data

Terrestrial sediments enjoy many of the same advantages as marine sediments for paleomagnetic reconstruction, particularly the ability to provide continuous records over long periods of time. However, they are also subject to the same uncertainties as marine sediments (i.e., debate over the interpretation of the post-DRM signal, potential chronologic inaccuracies, smoothing of high-frequency variations, and sediment deformation during coring).

Ohno and Hamano [20,21] used the paleoinclination and declination in a series of 10 sediment cores and two long archeomagnetic data sets to reconstruct the position and movement of the geomagnetic pole over the last 10 ka. Cores were chosen for analysis based on the following criteria: (1) the RM of the sediments was stable, (2) the chronology of each core was based on at least five radiocarbon ages, and (3) the average sedimentation rate exceeded 0.4 mm year^{-1}. The raw inclination and declination data obtained from the sediment cores were first compared to archeomagnetic and/or paleomagnetic data from nearby sites, if available. Such independent data was only available for four of the cores. The four cores were consistent with these data, and thus no corrections were necessary. The remaining cores were compared to a second-order spherical harmonic model of a global set of archeomagnetic and paleomagnetic data extending from 0.35 to 1.55 ka. The measured core data were corrected for time lags (up to 400 years) and deviation of the measured inclination from the modeled value (up to 5°). The average position of the VGP was then calculated at 100-year time intervals based on the corrected sediment core and archeomagnetic inclination and declination data.

3.2.3. Treatment of geomagnetic pole position data

Archeomagnetic and terrestrial sediment data pertaining to the position of the geomagnetic pole were originally reported as latitude and longitude at 100-year intervals [18–21]. We used the archeomagnetic data of Merrill and McElhinny [19] exclusively for the last 2 ka and the lacustrine sediment and archeomagnetic data of Ohno and Hamano [20,21] between 2 and 10 ka. Although these data sets are independent, we did not combine them because we believe that Merrill and McElhinny's [19] data set is superior to that of Ohno and Hamano [20,21] for several reasons. First, TRM data in archeomagnetic material are better understood and generally more reliable than post-DRM data in terrestrial sediments [35,50]. Second, VGP positions from Merrill and McElhinny [19] are average values from up to eight regions, each based on multiple measurements from a number of sites within each region. In contrast, VGP positions from Ohno and Hamano [20,21] are based

on a maximum of 12 data sets, each essentially acting as a single site. Furthermore, data from all 12 of these sites are only available to 4 ka, and only six data sets extend back to 10 ka. Finally, it was difficult to evaluate the accuracy of the post-DRM record of Ohno and Hamano [20,21] because measurement uncertainties in the data were ignored in their analysis and potential biases in the method used to correct the data were not rigorously addressed.

Since we lack geomagnetic pole position information beyond the Holocene, we must assume a GAD prior to 10 ka. The time period required for the geomagnetic field to average effectively to a GAD is still uncertain, but is generally thought to be between 10 and 100 ka [13,26]. Although the geomagnetic pole was generally within 5–10° latitude of the geographic pole through the Holocene, this is not necessarily characteristic of its long-term variation [35] and polar wander effects on CN production in the late Pleistocene could potentially be significant. CN research would clearly benefit from further work to extend the polar wander record.

4. Calculating time-integrated in situ CN production rates

Three steps are required for calculating site-specific, time-integrated in situ CN production rates: (1) determine the modern in situ CN production rate at SLHL, (2) account for spatial variation in the secondary cosmic-ray flux by scaling the modern production rate at SLHL to the site of interest, and (3) account for temporal variations in the geomagnetic field (intensity and polar wander). We simplified the first step by assuming a modern production rate of 1 atom g^{-1} $year^{-1}$ at SLHL. To account for spatial variation in the secondary cosmic-ray flux, we used the scaling model of Desilets and Zreda [1]. We selected this model because it is based on cosmic-ray survey data that are ordered by R_c values derived by numerically tracing the trajectories of thousands of incoming particles in a high-order geomagnetic field model. This is recognized as the most accurate method for ordering cosmic ray survey data, and virtually all cosmic-ray surveys since the 1960s utilize trajectory-traced R_c values (e.g., [51]). In addition, Desilets and Zreda [1] is the only published study with separate scaling models for the cosmic-ray particles (high- and low-energy nucleons, fast and slow muons) primarily responsible for CN production. The temporal scaling model presented here can incorporate other spatial scaling models, but the primary purpose of this study was to isolate and evaluate the effects of temporal variations in the Earth's geomagnetic field on integrated in situ ^{14}C and ^{10}Be production. This is best accomplished by using only one spatial scaling model, regardless of which one is chosen, thereby eliminating complications due to inherent differences between models. (Note that for comparison we also modeled the impact of geomagnetic variations on CN production using the spatial scaling models of Dunai [26] and Stone [14]. The overall spatial patterns of integrated CN production were similar, although individual results were up to 12 and 24% lower, respectively, relative to Desilets and Zreda [1].)

We accounted for temporal variations in the geomagnetic field as follows. First, we used the reported latitude and longitude positions of the VGP (Section 3.2.3) to calculate the geomagnetic colatitude of a given site (assuming a geocentric dipole) at 100-year time intervals over the chosen duration of exposure within the Holocene (Appendix A, Eq. (1)). We then used the corresponding geomagnetic latitude and normalized dipole moment (M/M_0) value (Section 3.1.3) to determine the R_c at the site, also at 100-year intervals (Appendix A, Eq. (2)). This required interpolation of the paleointensity data, assuming a linear variation between data points originally reported in 0.5 or 1 ka intervals. The VGP data were already reported in 100-year intervals. We used the 1-ka intervals of the SINT-800 data set directly beyond 50 ka.

We used the R_c value and site altitude to calculate effective attenuation lengths (Appendix A, Eq. (3)), and altitudinal and latitudinal scaling factors (Appendix A, Eqs. (4) and (5), respectively) at each time interval for high-energy nucleons, fast muons, and slow muons. The altitudinal and latitudinal scaling factors were combined to yield a total scaling factor for each reaction pathway (Appendix A, Eq. (6)). The resulting scaling factors were combined with the production proportions for each pathway as determined by Heisinger et al. [52] (Appendix A, Eq. (7)) and summed to determine the total production rate for each time interval. The inte-

grated in situ CN production rate was calculated as the weighted mean of the total production rate for each time interval averaged over the exposure duration, weighted by decay of the CN used and the inverse squared relative uncertainty in the total production rate (Appendix A, Eq. (8)). It is important to note that our decay clock runs from the time of the initial exposure to the present, not vice versa. While less important for longer-lived and stable nuclides, this distinction is critical for in situ ^{14}C. The result is a time-integrated, site-specific in situ CN production rate that accounts for spatial and temporal variations in the geomagnetic field. A geomagnetic correction factor for a given site and exposure interval was then derived by normalizing the integrated production rate to the modern production rate at the geomagnetic latitude of that site, referenced to the 1945.0 DGRF (Appendix A, Eq. (9)).

5. Model results

We modeled the global effects of geomagnetic variations on integrated production of both in situ ^{14}C and ^{10}Be by varying the following parameters: latitude in 5° increments between −90° and 90°, longitude in 15° increments between 0° and 360°, altitude in 1000-m increments between sea level and 4000 m, and exposure time in 1-ka increments between 0 and 20 ka and in 5-ka increments between 20 and 150 ka. We focus the discussion below on production at sea level because although the difference between integrated and modern production rates increases significantly with altitude (up to 19% greater at 4000 m), the spatial patterns of CN production are similar. We investigate separately the impacts of variations in geomagnetic intensity (assuming a GAD for the calculations) and polar wander on integrated CN production, followed by a discussion of their combined impact. All uncertainties are reported at the 1σ level (Appendix A).

5.1. Impact of variations in geomagnetic field intensity

The influence of variations in the intensity of the Earth's geomagnetic field on in situ CN production depends on the nuclide used, as well as the site latitude and exposure time. During the Holocene, the maximum effect for both nuclides occurs over the last 3 ka of exposure. For samples exposed at low geomagnetic latitudes (0–20°) for the last 3 ka, intensity-corrected in situ ^{14}C production rates are ~11% (~13% for ^{10}Be) lower than modern rates at the same site. At midlatitudes (30–40°), the difference between intensity-corrected and modern ^{14}C production rates decreases to 6–9% (7–11% for ^{10}Be). Geomagnetic intensity variations have no effect on CN production at geomagnetic latitudes >60°.

The impact of intensity variations on integrated CN production decreases steadily with increasing age, becoming insignificant for samples exposed for the last 20 ka, regardless of geomagnetic latitude. Intensity-corrected ^{14}C production rates integrated over this period at low and midlatitudes are <2% below modern, while corresponding intensity-corrected ^{10}Be production rates are 3–4% above modern (intensity-corrected ^{10}Be production exceeds the modern rate after about 15 ka).

The influence of geomagnetic field intensity variations on samples exposed for more than the last 20 ka is significant for long-lived CNs, but not for in situ ^{14}C. Intensity-corrected ^{14}C production rates are within 3% of modern rates for samples that have been exposed for the last 50 ka, whereas integrated ^{10}Be rates are up to ~30% higher than modern under the same conditions. The reason for this difference is that the short half-life of ^{14}C results in greater weight being given to the most recent time periods. For example, if a landform has been continually exposed at the Earth's surface for the last 50 ka, only ~0.2% of in situ ^{14}C atoms produced at the initial time of exposure remain at the time of measurement. In contrast, ~97% of ^{10}Be atoms produced at the initial time of exposure remain under the same conditions—even after 800 ka, ~70% of the originally produced ^{10}Be atoms remain. Therefore, atoms produced more recently dominate the in situ ^{14}C inventory, whereas the ^{10}Be inventory represents all time periods more or less equally over the same duration. The result is that integrated ^{10}Be production rates closely follow the integrated geomagnetic field intensity record for the last 40 ka, whereas integrated ^{14}C rates are skewed toward the present.

5.2. Impact of polar wander

The maximum impact of polar wander at a given latitude is observed along a plane defined by the 105° and 285° meridians (Fig. 2). The longitudinal position of a site is important because motion of the geomagnetic pole along a plane rapidly changes the geomagnetic latitude (and R_c) of sites located along the same plane. Motion of the pole does not affect production at sites positioned along a meridian perpendicular to the plane of motion. Geomagnetic polar motion over the past several thousand years has been primarily from north to south near the 105° meridian and therefore, production rates that account for polar wander generally increase near 105° longitude in the northern hemisphere (285° longitude in the southern hemisphere) and decrease near 285° longitude in the northern hemisphere (105° longitude in the southern hemisphere). CN production at sites located along the 15–195° meridian, which is perpendicular to the plane of polar motion, has not been significantly affected by Holocene polar wander.

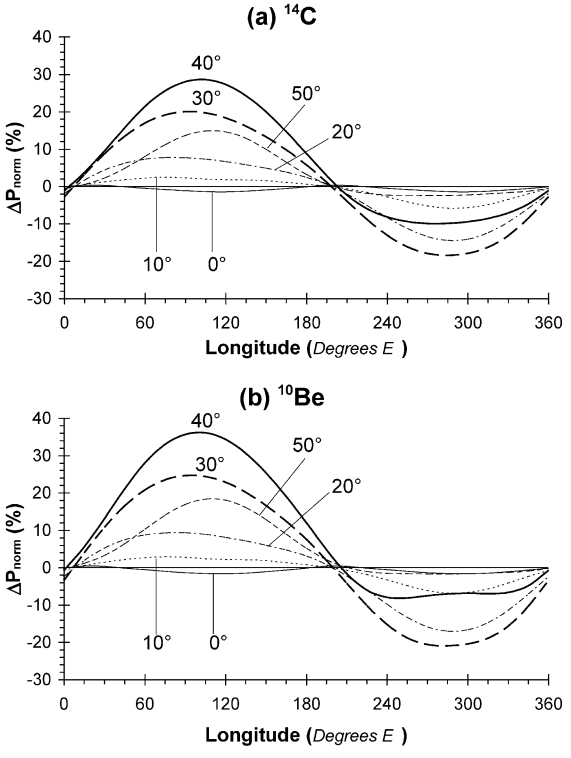

Fig. 2. Variation with longitude of the percent difference (ΔP_{norm}) between integrated production rates at sea level accounting only for polar wander and modern rates for (a) in situ ^{14}C and (b) in situ ^{10}Be for the last 5 ka. Note that for a given site, the integrated rate is normalized to the modern rate at the *geomagnetic* latitude of the site. The impact of polar wander on integrated production rates is highest at midlatitudes (30–40°) along a plane defined by the 105° and 285° meridians. The unmarked thin solid lines represent modern production rates.

Polar wander does not significantly affect integrated CN production rates at either low (0–15°) or high (>60°) latitudes, regardless of the nuclide used. At these latitudes, integrated ^{14}C and ^{10}Be rates that account only for polar wander (M/M_0=1 during exposure) are within ~5% of modern rates (Fig. 2). The impact of polar wander is much greater at midlatitudes (30–40°) where integrated in situ ^{14}C rates that account only for polar wander are between ~29% higher and 19% lower (~36% higher and 21% lower for ^{10}Be) than modern for samples exposed for the last 5 ka, depending on the site longitude.

The maximum impact of polar wander is observed for samples exposed for approximately the last 5 ka, but the influence of polar wander decreases only slightly with increasing exposure time. For example, the difference between integrated in situ ^{14}C rates that account for polar wander and modern rates is still up to ~27% higher and 19% lower (~30% higher and 22% lower for ^{10}Be) at midlatitudes even after 50 ka of exposure. This may seem counter to the commonly held notion that polar wander is not important for samples exposed for >10–15 ka. However, this simply reflects our normalization of the integrated production rate at a given site to the modern rate at that site's geomagnetic latitude, which accounts for the current separation between the geomagnetic and geographic poles. The 1945.0 DGRF geomagnetic pole is 11.5° latitude from the geographic pole, while the separation between the poles was <5° latitude for most of the Holocene [18–21].

5.3. Combined impact of intensity variations and polar wander

Integrated production rates during the Holocene that account for both polar wander and intensity

variations, but which have not been normalized to the modern rate, are within 5% of those corrected only for intensity variations, regardless of site location, duration of exposure, or nuclide used. When normalized to the modern rate at the geomagnetic latitude of a given site, however, integrated in situ ^{14}C rates accounting for both polar wander and intensity fluctuations are between 22% higher and 24% lower (28% higher and 26% lower for ^{10}Be) than modern for samples exposed for the last 5 ka (Figs. 3 and 4). The difference between integrated and modern in situ ^{14}C rates increases only slightly with increasing exposure time (Figs. 3 and 4). In contrast, the difference between integrated and modern in situ ^{10}Be rates increases dramatically with longer exposure times, and are up to 50% higher than modern for samples exposed for the last 50 ka (Figs. 3 and 4). Beyond 50 ka, the integrated

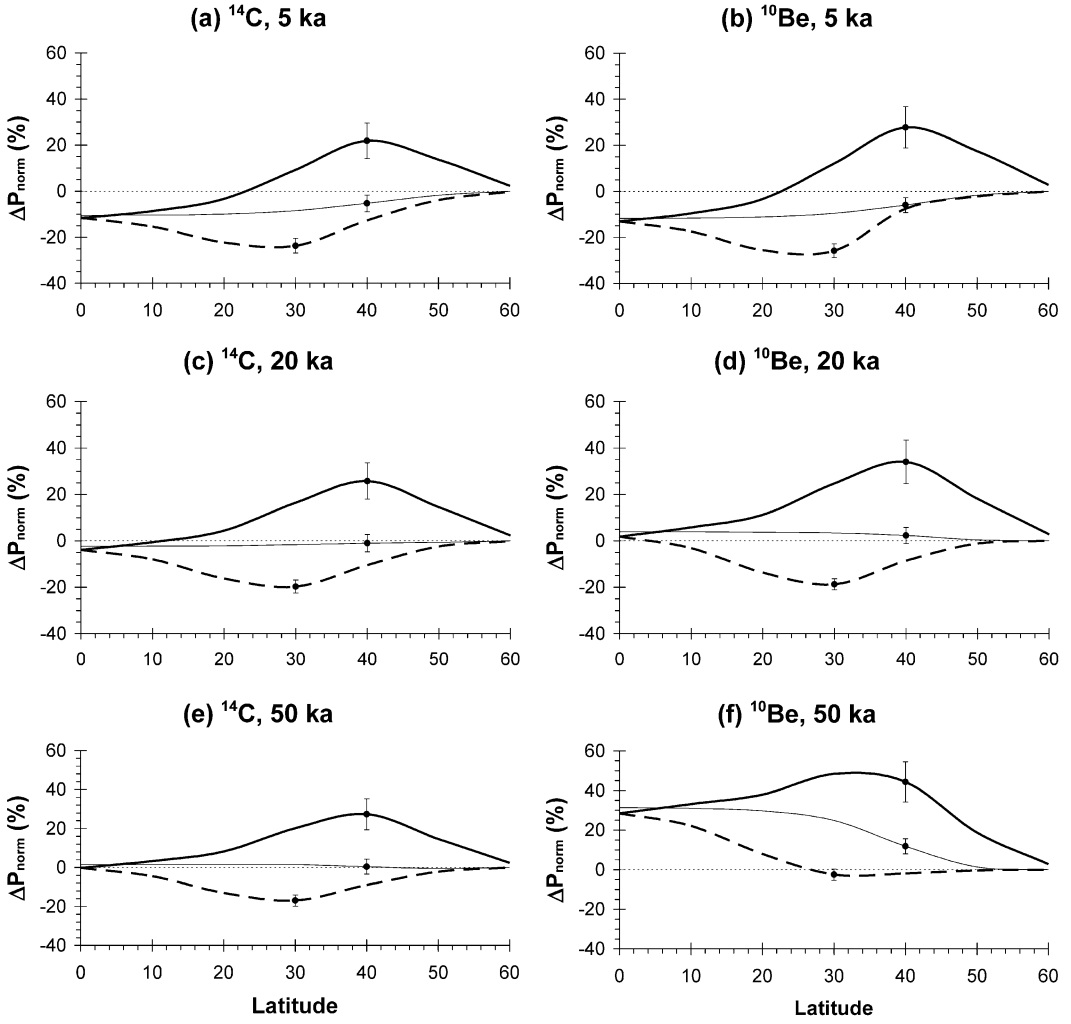

Fig. 3. Variation with geographic latitude of ΔP_{norm} values at 105° longitude (thick solid lines) and 285° longitude (thick dashed lines) for integrated in situ ^{14}C (a, c and e) and ^{10}Be (b, d and f) production rates at sea level accounting for both intensity variations and polar wander, for different exposure times. Production rates at all other latitudes fall within these two extremes. Also shown are integrated production rates that are incorrectly normalized to the *geographic* latitude of a site (thin solid line), which could lead to errors of as much as ±25–30% at sea level. Thin dotted lines represent modern production rates.

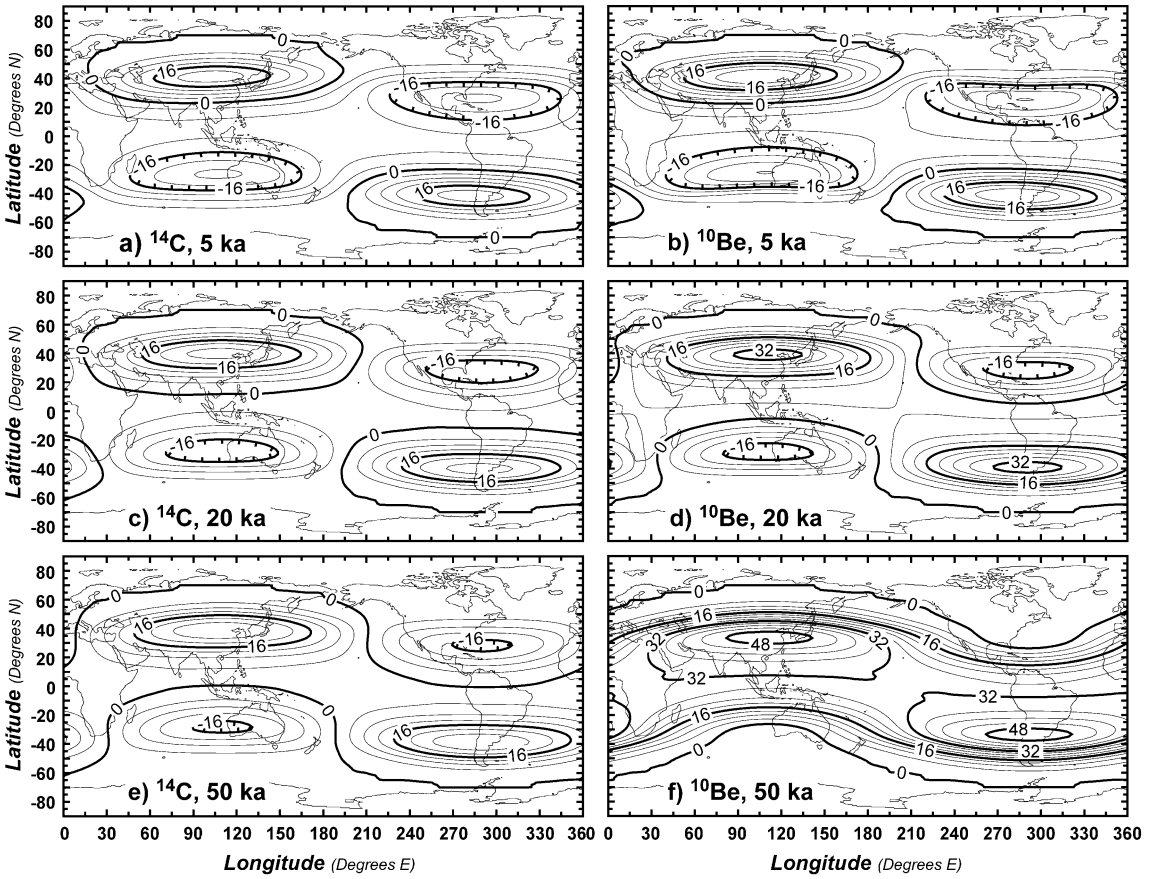

Fig. 4. Global maps depicting ΔP_{norm} values for in situ ^{14}C (a, c and e) and in situ ^{10}Be (b, d and f) production rates accounting for both intensity variations and polar wander, for different exposure times. The impact of geomagnetic field intensity variations on samples exposed for more than the last 20 ka diverges for short- and long-lived CNs because the relatively short half-life of ^{14}C results in greater weight being given to the most recent time periods, whereas minimal decay of the ^{10}Be inventory weights all time intervals more or less equally over the exposure durations depicted here. Contour interval is 4%.

production rates remain within 5% of these values over the last 800 ka.

6. Conclusions

The impact of correcting modern production rates for temporal variations in the Earth's geomagnetic field intensity and movement of the geomagnetic pole depends on the site location, altitude, exposure duration, and nuclide used. This paper presents a consistent framework for incorporating the effects of these variations on time-integrated CN production rates. To stimulate debate of how best to incorporate geomagnetic variations into time-integrated production rates, we have discussed the merits and limitations of using specific geomagnetic records and the treatment of the paleomagnetic data, and have provided a copy of our model as a Microsoft Excel® template for general use (Appendix B). Our motivation in providing this spreadsheet is to encourage the reader to use the model to obtain accurate correction factors rather than attempting to approximate a correction factor for a particular site or time interval from Fig. 3 or 4.

The impact of temporal variations in the geomagnetic field on CN production rates has often been ignored in CN applications. However, we have shown that this can lead to significant errors in the time-integrated production rate experienced by a given sample, and thus in the interpretation of that sample's

exposure history. We have also shown that it is critical to normalize time-integrated production rates to the modern production rate (referenced to a specific geomagnetic reference field) at the geomagnetic, rather than geographic, latitude of a site. Normalizing integrated production rates to modern rates using the site's geographic latitude (i.e., assuming a GAD) can lead to errors in the correction factor of up to ±25–30% at sea level. We thus recommend correcting the modern production rate (referenced to the 1945.0 DGRF or another specific geomagnetic reference field) at site latitudes <60° for variations in the intensity of the Earth's geomagnetic field during exposure, and for polar wander over the last 10 ka.

Acknowledgements

We thank J. Wilson for modeling assistance and R. Butler for insightful conversations. We also thank Bill Phillips and Joerg Schaefer for their thoughtful reviews. This work was supported by NSF Grant EAR-0001069 and by the NSF-Arizona Accelerator Mass Spectrometry Facility.

Appendices A and B. Supplementary data

Supplementary data associated with this article can be found, in the online version, at doi:10.1016/j.epsl.2004.07.031.

References

[1] D. Desilets, M. Zreda, Spatial and temporal distribution of secondary cosmic-ray nucleon intensities and applications to in situ cosmogenic dating, Earth Planet. Sci. Lett. 206 (2003) 21–42.

[2] D.E. Granger, J.W. Kirchner, R. Finkel, Spatially averaged long-term erosion rates measured from in situ-produced cosmogenic nuclides in alluvial sediment, J. Geol. 104 (1996) 249–257.

[3] E.E. Small, R.S. Anderson, J.L. Repka, R. Finkel, Erosion rates of alpine bedrock summit surfaces deduced from in situ ^{10}Be and ^{26}Al, Earth Planet. Sci. Lett. 150 (1997) 413–425.

[4] P.R. Bierman, M. Caffee, Slow rates of rock surface erosion and sediment production across the Namib Desert and escarpment, southern Africa, Am. J. Sci. 301 (2001) 326–358.

[5] J.W. Kirchner, R.C. Finkel, C.S. Riebe, D.E. Granger, J.L. Clayton, J.G. King, W.F. Megahan, Mountain erosion over 10 yr, 10 ky, and 10 my time scales, Geology 29 (2001) 591–594.

[6] J.C. Gosse, J. Klein, E.B. Evenson, B. Lawn, R. Middleton, Beryllium-10 dating of the duration and retreat of the last Pinedale glacial sequence, Science 268 (1995) 1329–1333.

[7] F.M. Phillips, M.G. Zreda, L.V. Benson, M.A. Plummer, D. Elmore, P. Sharma, Chronology for fluctuations in Late Pleistocene Sierra Nevada glaciers and lakes, Science 274 (1996) 749–751.

[8] L.A. Owen, R.C. Finkel, R.A. Minnich, A.E. Perez, Extreme southwestern margin of late Quaternary glaciation in North America: timing and controls, Geology 31 (2003) 729–732.

[9] M.G. Zreda, F.M. Phillips, P.W. Kubik, P. Sharma, D. Elmore, Cosmogenic ^{36}Cl dating of a young basaltic eruption complex, Lathrop Wells, Nevada, Geology 21 (1993) 57–60.

[10] F.M. Phillips, Cosmogenic ^{36}Cl ages of Quaternary basalt flows in the Mojave Desert, California, USA. Geomorphology 53 (2003) 199–208.

[11] M. Zreda, J.S. Noller, Ages of prehistoric earthquakes revealed by cosmogenic chlorine-36 in a bedrock fault scarp at Hebgen Lake, Science 282 (1998) 1097–1099.

[12] F.M. Phillips, J.P. Ayarbe, J.B.J. Harrison, D. Elmore, Dating rupture events on alluvial fault scarps using cosmogenic nuclides and scarp morphology, Earth Planet. Sci. Lett. 215 (2003) 203–218.

[13] J.C. Gosse, F.M. Phillips, Terrestrial in situ cosmogenic nuclides: theory and application, Quat. Sci. Rev. 20 (2001) 1475–1560.

[14] J.O. Stone, Air pressure and cosmogenic isotope production, J. Geophys. Res. 105 (2000) 23,753–23,759.

[15] Y. Guyodo, J.P. Valet, Relative variations in geomagnetic intensity from sedimentary records: the past 200,000 years, Earth Planet. Sci. Lett. 143 (1996) 23–36.

[16] Y. Guyodo, J.-P. Valet, Global changes in intensity of the Earth's magnetic field during the past 800 kyr, Nature 399 (1999) 249–252.

[17] S. Yang, H. Odah, J. Shaw, Variations in the geomagnetic dipole moment over the last 12,000 years, Geophys. J. Int. 140 (2000) 158–162.

[18] D.E. Champion, Holocene geomagnetic secular variation in the western United States: implications for the global geomagnetic field, Open-File Rep. (U. S. Geol. Surv.) 80-824 (1980) 314.

[19] R.T. Merrill, M.W. McElhinny, The Earth's Magnetic Field: Its History, Origin, and Planetary Perspective, Academic Press, London, 1983, 401 pp.

[20] M. Ohno, Y. Hamano, Geomagnetic poles over the past 10,000 years, Geophys. Res. Lett. 19 (1992) 1715–1718.

[21] M. Ohno, Y. Hamano, Global analysis of the geomagnetic field: time variation of the dipole moment and the geomagnetic pole in the Holocene, J. Geomag. Geoelectr. 45 (1993) 1455–1466.

[22] E. Clapp, P.R. Bierman, COSMO-CALIBRATE: a program for calibrating cosmogenic exposure ages, in: J.C. Gosse, R.C. Reedy, C.D. Harrington, J. Poths (Eds.), Workshop on Secular Variations in Production Rates of Cosmogenic Nuclides on Earth, Santa Fe, NM, Radiocarbon, vol. 38, 1996, pp. 151–152.

[23] J. Klein, J. Gosse, Terrestrial factors that influence production rates, in: J. Gosse, R.C. Reedy, C.D. Harrington, J. Poths (Eds.), Workshop on Secular Variations, Santa Fe, NM, Radiocarbon, vol. 38, 1996, pp. 161–162.
[24] J.M. Licciardi, M.D. Kurz, P.U. Clark, E.J. Brook, Calibration of cosmogenic ^{3}He production rates from Holocene lava flows in Oregon, USA, and effects of the Earth's magnetic field, Earth Planet. Sci. Lett. 172 (1999) 261–271.
[25] T.M. Shanahan, M. Zreda, Chronology of Quaternary glaciations in East Africa, Earth Planet. Sci. Lett. 177 (2000) 23–42.
[26] T.J. Dunai, Influence of secular variation of the geomagnetic field on production rates of in situ produced cosmogenic nuclides, Earth Planet. Sci. Lett. 193 (2001) 197–212.
[27] J. Masarik, M. Frank, J.M. Schäfer, R. Wieler, Correction of in situ cosmogenic nuclide production rates for geomagnetic field intensity variations during the past 800,000 years, Geochim. Cosmochim. Acta 65 (2001) 2995–3003.
[28] B. Rossi, Interpretation of cosmic-ray phenomena, Rev. Mod. Phys. 20 (1948) 537–583.
[29] T.K. Gassier, Cosmic Rays and Particle Physics, Cambridge University Press, Cambridge, MA, 1990, 279 pp.
[30] J. Masarik, J. Beer, Simulation of particle fluxes and cosmogenic nuclide production in the Earth's atmosphere, J. Geophys. Res. 104 (1999) 12,099–12,111.
[31] G. Castagnoli, D. Lal, Solar modulation effects in terrestrial production of carbon-14, Radiocarbon 22 (1980) 133–158.
[32] J.F. Ziegler, Terrestrial cosmic rays, IBM J. Res. Develop. 40 (1996) 19–39.
[33] A. Belov, Large scale modulation: view from the Earth, Space Sci. Rev. 93 (2000) 79–105.
[34] D.J. Cooke, J.E. Humble, M.A. Shea, D.F. Smart, N. Lund, I.L. Rasmussen, B. Byrnak, P. Goret, N. Petrou, On cosmic-ray cut-off terminology, Nuovo Cim., Ser. C 14 (1991) 213–234.
[35] R.T. Merrill, M.W. McElhinny, P.L. McFadden, The Magnetic Field of the Earth: Paleomagnetism, the Core, and the Deep Mantle, Academic Press, London, 1996, 531 pp.
[36] D. Lal, B. Peters, Cosmic ray produced radioactivity on the Earth, in: K. Sitte (Ed.), Handbuch Der Physik, vol. XLVI/2, Springer-Verlag, Berlin, 1967, pp. 551–612.
[37] D. Lal, Cosmic ray labeling of erosion surfaces: in situ nuclide production rates and erosion models, Earth Planet. Sci. Lett. 104 (1991) 424–439.
[38] T.J. Dunai, Scaling factors for production rates of in situ produced cosmogenic nuclides: a critical reevaluation, Earth Planet. Sci. Lett. 176 (2000) 157–169.
[39] M.W. McElhinny, W.E. Senanayake, Variations in the geomagnetic dipole 1: the past 50,000 years, J. Geomag. Geoelectr. 34 (1982) 39–51.
[40] M. Frank, B. Schwarz, S. Baumann, P.W. Kubik, M. Suter, A. Mangini, A 200 kyr record of cosmogenic radionuclide production rate and geomagnetic field intensity from Be-10 in globally stacked deep-sea sediments, Earth Planet. Sci. Lett. 149 (1997) 121–129.
[41] M. Frank, Comparison of cosmogenic radionuclide production and geomagnetic field intensity over the last 200,000 years, Philos. Trans. R. Soc. Lond. Ser. A: Math. Phys. Sci. 358 (2000) 1089–1107.
[42] C. Laj, A. Mazaud, J.C. Duplessy, Geomagnetic intensity and ^{14}C abundance in the atmosphere and ocean during the past 50 kyr, Geophys. Res. Lett. 23 (1996) 2045–2048.
[43] J.W. Beck, D.A. Richards, R.L. Edwards, B.W. Silverman, P.L. Smart, D.J. Donahue, S. Hererra-Osterheld, G.S. Burr, L. Calsoyas, A.J.T. Jull, D. Biddulph, Extremely large variations of atmospheric ^{14}C concentration during the last glacial period, Science 292 (2001) 2453–2458.
[44] K. Hughen, S. Lehman, J. Southon, J. Overpeck, O. Marchal, C. Herring, J. Turnbull, ^{14}C activity and global carbon cycle changes over the past 50,000 years, Science 303 (2004) 202–207.
[45] U. Siegenthaler, J.L. Sarmiento, Atmospheric carbon dioxide and the ocean, Nature 365 (1993) 119–125.
[46] M. Stuiver, P.J. Reimer, E. Bard, J.W. Beck, G.S. Burr, K.A. Hughen, B. Kromer, G. McCormick, J. van der Plicht, M. Spurk, INTCAL98 radiocarbon age calibration, Radiocarbon 40 (1998) 1041–1083.
[47] D.G. Martinson, N.G. Pisias, J.D. Hays, J. Imbrie, T.C. Moore Jr., N.J. Shackleton, Age dating and the orbital theory of the ice ages: development of a high-resolution 0 to 300,000-yr chronostratigraphy, Quat. Res. 27 (1987) 1–29.
[48] N. Thouveny, K.M. Creer, D. Williamson, Geomagnetic moment variations in the last 70,000 years, impact on production of cosmogenic isotopes, Glob. Planet. Change 7 (1993) 157–172.
[49] H. Tanaka, A. Otsuka, T. Tachibana, M. Kono, Some global features of palaeointensity in geological time, Geophys. J. Int. 120 (1994) 97–102.
[50] R.F. Butler, Paleomagnetism: Magnetic Domains to Geologic Terranes, Blackwell Scientific Publishers, Boston, MA, 1992, 319 pp.
[51] O.C. Allkofer, P.K.F. Grieder, Cosmic rays on Earth, Phys. Data 25 (1984) 1–379.
[52] B. Heisinger, D. Lal, A.J.T. Jull, P. Kubik, S. Ivy-Ochs, K. Knie, E. Nolte, Production of selected cosmogenic radionuclides by muons: 2. Capture of negative muons, Earth Planet. Sci. Lett. 200 (2002) 357–369.